

# Depletion induced isotropic-isotropic phase separation in suspensions of rod-like colloids

S. Jungblut

*Institut für Physik, Johannes Gutenberg-Universität, Staudinger Weg 7, D-55099 Mainz, Germany*

R. Tuinier

*Forschungszentrum Jülich, Institut für Festkörperforschung, D-52425 Jülich, Germany*

K. Binder and T. Schilling<sup>a)</sup>

*Institut für Physik, Johannes Gutenberg-Universität, Staudinger Weg 7, D-55099 Mainz, Germany*

(Received 3 August 2007; accepted 29 October 2007; published online 28 December 2007)

When non-adsorbing polymers are added to an isotropic suspension of rod-like colloids, the colloids effectively attract each other via depletion forces. We performed Monte Carlo simulations to study the phase diagram of such rod-polymer mixture. The colloidal rods were modeled as hard spherocylinders; the polymers were described as spheres of the same diameter as the rods. The polymers may overlap with no energy cost, while the overlap of polymers and rods is forbidden. Large amounts of depletant cause phase separation of the mixture. We estimated the phase boundaries of isotropic-isotropic coexistence both in the bulk and in confinement. To determine the phase boundaries we applied the grand canonical ensemble using successive umbrella sampling [J. Chem. Phys. **120**, 10925 (2004)], and we performed a finite size scaling analysis to estimate the location of the critical point. The results are compared with predictions of the free volume theory developed by Lekkerkerker and Stroobants [Nuovo Cimento D **16**, 949 (1994)]. We also give estimates for the interfacial tension between the coexisting isotropic phases and analyze its power-law behavior on the approach of the critical point. © 2007 American Institute of Physics. [DOI: 10.1063/1.2815805]

## I. INTRODUCTION

Non-adsorbing polymers are often added to colloidal suspensions in order to modify the effective interactions between the colloids. By this means phase transitions can be driven, e.g., in order to facilitate the isolation of the colloids.<sup>1</sup> In particular, mixtures of viruses and polymers are widely used in experiments on colloidal liquid crystals (see, for instance, the recent review by Dogic and Fraden<sup>2</sup>).

As certain viruses, such as tobacco mosaic virus and fd-virus, can to a first approximation be regarded as long cylinders, they are good model systems for liquid crystals. Currently there is much interest in the nonequilibrium behavior of these systems, in particular, in the effect of shear.<sup>3–6</sup> In order to interpret the experimental results, detailed theoretical knowledge on the equilibrium phase diagram is needed. Therefore we present in this article a computer simulation study of the phase behavior of rods and spheres, both in the bulk and in confinement.

The Asakura-Oosawa-Vrij model<sup>7,8</sup> is a useful model for mixtures of polymers and spherical colloids. The polymers are assumed to be freely interpenetrable with respect to each other, while there is a hard-core repulsion between the colloids as well as between the colloids and the polymers. As the interaction energy is then either zero or infinite, the phase behavior is purely of entropic origin.

In this article we discuss a similar model for mixtures of

rod-like colloids and polymers: a mixture of hard spherocylinders with length  $L$  and diameter  $D$  and freely interpenetrable spheres with the same diameter.

This system was studied with the liquid-state integral equation theory<sup>9–11</sup> and the free volume theory<sup>12</sup> as well as with computer simulations.<sup>13–15</sup> In recent years various regimes of size-ratios and concentrations have been discussed, e.g., the packing properties at very high concentrations or the behavior of small rods, which act as a depletant on large spheres. Here we focus on dispersions of rods and spheres of similar diameters at low concentrations. The phase diagram of this model was studied within the free volume theory by Lekkerkerker and Stroobants.<sup>12</sup> Details of this approach will be described in Sec. II. Li and Ma recently computed the effective interaction between two rods by Monte Carlo simulation.<sup>13</sup> Bolhuis *et al.*<sup>14</sup> as well as Savenko and Dijkstra<sup>15</sup> determined the bulk rod-sphere phase diagram by simulation (via thermodynamic integration). Both have given results for rods of aspect ratio  $L/D=5$  and spheres of several diameter values. In order to avoid simulating the spheres explicitly, Savenko and Dijkstra used an exact expression for the effective Hamiltonian, which was numerically evaluated during the Monte Carlo simulation for each rod configuration. Bolhuis *et al.*<sup>14</sup> modeled the spheres explicitly in their Gibbs Ensemble Monte Carlo simulations to study fluid-fluid separation, while for the other parts of the phase diagram they used an effective expression for the rod-rod interaction.

Here we present results for the full rod-sphere system, which were obtained in the grand canonical ensemble. The

<sup>a)</sup>Electronic mail: schillit@uni-mainz.de.

successive umbrella sampling method<sup>16</sup> was employed to determine the grand potential hypersurface of the system. This allowed us to predict the phase boundaries of isotropic-isotropic coexistence with much higher accuracy than the studies mentioned above, which used thermodynamic integration. In particular, we determined the critical point by a finite size scaling analysis. We also studied the influence of confinement on the phase behavior. This is relevant for experiments under shear.

In Sec. II we briefly review the free volume theory for the rod-sphere mixture. In Sec. III the simulation method is introduced. In Sec. IV we show results for phase diagrams and interfacial tensions and compare them to the theoretical predictions. Section V contains a summary and a discussion.

## II. FREE VOLUME THEORY

We briefly review the theoretical approach to rod-sphere mixtures which was introduced by Lekkerkerker and Stroobants<sup>12</sup> in 1994. The starting point is the thermodynamic potential in the semi-grand canonical ensemble, where the number of rods is fixed, while the number of “penetrable hard” spheres is set by the chemical potential of spheres in a hypothetical reservoir that is held in equilibrium with the system. The potential  $\Omega^{\text{semi}}(N_r, V, T, \text{ and } \mu_s)$  of such a mixture can be written as

$$\begin{aligned}\Omega^{\text{semi}} &= F(N_r, V, T) + \int_{-\infty}^{\mu_s^R} \frac{\partial \Omega(N_r, V, T, \mu_s'^R)}{\partial \mu_s'^R} d\mu_s'^R \\ &= F(N_r, V, T) - \int_{-\infty}^{\mu_s^R} N_s(\mu_s'^R) d\mu_s'^R,\end{aligned}\quad (1)$$

where  $F(N_r, V, T)$  is the free energy of  $N_r$  rods in a volume  $V$  at temperature  $T$ , and the second term accounts for the perturbation due to the addition of  $N_s$  spheres from a reservoir, where the chemical potential is kept at  $\mu_s^R$ . Osmotic equilibrium requires the chemical potentials of the system and the reservoir to be equal. The chemical potential of an ideal gas of spheres is connected to the density  $\rho_s$  via

$$\rho_s = \exp\left(\frac{\mu_s}{k_B T}\right).\quad (2)$$

Thus, the number of spheres in the system depends on  $\mu_s^R$ . The only influence the rods have on the spheres is the reduction of the free volume,

$$N_s = \rho_s^R V_{\text{free}},\quad (3)$$

where  $V_{\text{free}}$  is the volume accessible for spheres under the assumption that the rod configurations are undistorted upon adding spheres and  $\rho_s^R$  is the number density of spheres in the reservoir. The free volume fraction  $\alpha$  is defined as

$$\alpha = \frac{V_{\text{free}}}{V},\quad (4)$$

and it can be calculated within scaled particle theory.<sup>12</sup> Hence, the expression for the semi-grand canonical potential is reduced to

$$\Omega^{\text{semi}} = F(N_r, V, T) - \alpha V k_B T \rho_s^R.\quad (5)$$

The chemical potential as well as the osmotic pressure  $\Pi_r$  of the rods in the mixture can be obtained from the following thermodynamic relationships:

$$\mu_r = \left(\frac{\partial \Omega^{\text{semi}}}{\partial N_r}\right)_V,\quad (6)$$

$$\Pi_r = -\left(\frac{\partial \Omega^{\text{semi}}}{\partial V}\right)_{N_r},\quad (7)$$

where  $v_r = \pi D^3(2 + 3L/D)/12$  is the volume of a spherocylinder of length  $L$  and diameter  $D$ .

The virial expansion of the free energy of a system of hard spherocylinders can be calculated using the scaled particle theory,<sup>17</sup>

$$\frac{F v_r}{k_B T V} = \frac{y}{y+1} \left( \text{const} + \ln(y) + \sigma[f] + \Pi_2 y + \frac{\Pi_3}{2} y^2 \right),\quad (8)$$

with

$$y = \frac{\eta_r}{1 - \eta_r},\quad (9)$$

where  $\eta_r = \rho_r v_r$  is the volume fraction of rods.

$$\Pi_2 = 3 + \frac{3(\tau-1)^2}{3\tau-1} \rho[f],\quad (10)$$

$$\Pi_3 = \frac{12\tau(2\tau-1)}{(3\tau-1)^2} + \frac{12\tau(\tau-1)^2}{(3\tau-1)^2} \rho[f],$$

and  $\tau$  is the overall length-to-diameter ratio of the spherocylinders

$$\tau = \frac{L+D}{D}.\quad (11)$$

In Eqs. (8) and (10),  $\sigma[f]$  and  $\rho[f]$  are functionals of the orientational distribution function  $f$ ,

$$\sigma[f] = \int f(\mathbf{u}) \ln[4\pi f(\mathbf{u})] d\mathbf{u},\quad (12)$$

$$\rho[f] = \frac{4}{\pi} \int \int \sin[\Phi(\mathbf{u}, \mathbf{u}')] f(\mathbf{u}) f(\mathbf{u}') d\mathbf{u} d\mathbf{u}',\quad (13)$$

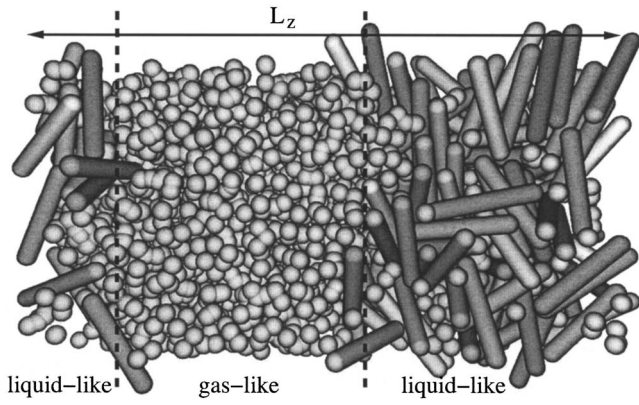
where  $\mathbf{u}$  is the unit vector along a particle's axis.

The normalized orientational distribution function of a single rod  $f$  is adapted to minimize the semi-grand canonical potential. In the nematic case it can be obtained either numerically<sup>18</sup> or from the Gaussian approximation,<sup>12</sup> but here we are interested in the isotropic case, i.e., all orientations  $\mathbf{u}$  are equally probable and the distribution is uniform,

$$f(\mathbf{u}) = \frac{1}{4\pi}.\quad (14)$$

Therefore, in our case, the functionals are reduced to

$$\sigma[f] = 0,\quad (15)$$

FIG. 1. Configuration snapshot for  $L/D=5$  at coexistence.

$$\rho[f] = 1. \quad (16)$$

The expression for the free volume fraction calculated with the scaled particle theory reads

$$\alpha = \frac{1}{1+y} e^{-(Ay+By^2+Cy^3)}, \quad (17)$$

where, in the isotropic case, for “penetrable hard” spheres with diameter  $D$ ,

$$A = \frac{6\tau}{3\tau-1} + \frac{3(\tau+1)}{3\tau-1} + \frac{2}{3\tau-1},$$

$$B = \frac{18\tau^2}{(3\tau-1)^2} + \left( \frac{6}{3\tau-1} + \frac{6(\tau-1)^2}{(3\tau-1)^2} \right), \quad (18)$$

$$C = \frac{2}{3\tau-1} \left( \frac{12\tau(2\tau-1)}{(3\tau-1)^2} + \frac{12\tau(\tau-1)^2}{(3\tau-1)^2} \right).$$

Thus, the chemical potential and the osmotic pressure of the rods in the mixture are functions of the rod volume fraction and of the chemical potential of spheres in the reservoir. At coexistence, they are equal. From this condition we have obtained the phase diagrams, which are compared to our simulation results in Sec. IV.

### III. MODEL AND SIMULATION METHOD

In our Monte Carlo simulations we model the colloids as hard spherocylinders of length  $L$  and diameter  $D$ . The polymers are approximated as spheres of the same diameter, which are hard with respect to the rods and freely interpenetrable among each other.

We performed simulations in the grand canonical ensemble, where the volume  $V$  and the chemical potentials  $\mu_r$  of the spherocylinders and  $\mu_s$  of the spheres are fixed. The temperature  $T$  is formally also fixed, but irrelevant, since it only sets the energy scale. Simulations were performed in a box with edges  $L_z \geq L_y = L_x \geq 3L$  and periodic boundary conditions. In a rectangular box configurations at coexistence form preferably such that the interfaces are parallel to the small faces of the box (see Fig. 1). This simplifies the analysis of the interfacial tension. The finite size effects were examined in a cubic box. For the study of confinement effects on our model system we choose a geometry where the box

dimensions were  $L_x=L_y \geq 3L$  and  $L_z=3L$  with periodic boundary conditions in the  $x$ - and  $y$ -directions and hard walls in the  $z$ -direction. To speed up the simulations we employed a cell system for efficient overlap detection of anisotropic particles.<sup>19</sup> In this approach the simulation box is cut into cubes of side lengths  $\geq D$ . Whether a rod intersects a cube or not can be computed very fast. The volume which needs to be checked for overlaps then contains at the most a few particles.

### A. Cluster move

In order to efficiently equilibrate canonical simulations of spherical colloids, Biben *et al.* introduced a cluster move.<sup>20</sup> Later this move was extended to simulations in the grand canonical ensemble.<sup>21</sup> Here we introduce a version that is adjusted to the case of spherocylinders.

If we attempt to insert a spherocylinder into a simulation box full of spheres, it will certainly overlap with some of them and the move will be rejected. The cluster move combines the insertion of a spherocylinder with the removal of the spheres, which it otherwise would overlap with. Thus it increases the probability of accepting an insertion move. At the same time, the removal of a spherocylinder is combined with the insertion of a certain amount of spheres in the void left by the removed spherocylinder.

Care has to be taken of the acceptance probabilities in order to ensure detailed balance. Here, we only give the most relevant equations. The reader who is interested in details is referred to the work by Vink and Horbach,<sup>21</sup> who have explained the process thoroughly for spherical colloids. For spherocylinders we have to account for an additional degree of freedom—the orientation. The Metropolis probability of accepting a removal of a spherocylinder in a cluster move is

$$\text{acc}(N_r \rightarrow N_r - 1) = \min \left[ 1, \frac{N_r m (z_s V_{dz})^{n_s}}{4\pi V z_r n_s!} e^{-\beta \Delta E} \right], \quad (19)$$

where  $\Delta E$  is the potential-energy difference between the initial and the final configurations—which is infinite for an overlapping configuration and zero otherwise. The volume of the depletion zone around a spherocylinder is  $V_{dz} = \pi(2D)^3(3L/(2D)+2)/12$ . The factors  $1/(4\pi)$  in Eq. (19) and  $4\pi$  in Eq. (21) are due to the orientational degree of freedom. The fugacities  $z_{r/s}$  of spherocylinders and spheres, respectively, are related to the chemical potentials via  $z_{r/s} = \exp(\beta \mu_{r/s})$ , where  $\beta = 1/(k_B T)$  is the inverse temperature.  $n_s$  is the number of spheres to be inserted into the void.  $n_s$  is drawn uniformly from the interval  $[0, m]$ , where  $m$  is an integer given by  $m = 1 + \max[1, \text{int}(z_s V_{dz} + a \sqrt{z_s V_{dz}})]$ , with  $a$  a positive constant of order unity.

If only one spherocylinder is removed and no spheres are inserted, the acceptance probability is reduced to

$$\text{acc}(N_r \rightarrow N_r - 1) = \min \left[ 1, \frac{N_r}{4\pi V z_r} e^{-\beta \Delta E} \right]. \quad (20)$$

The Metropolis probability of accepting an insertion of a spherocylinder in a cluster move is

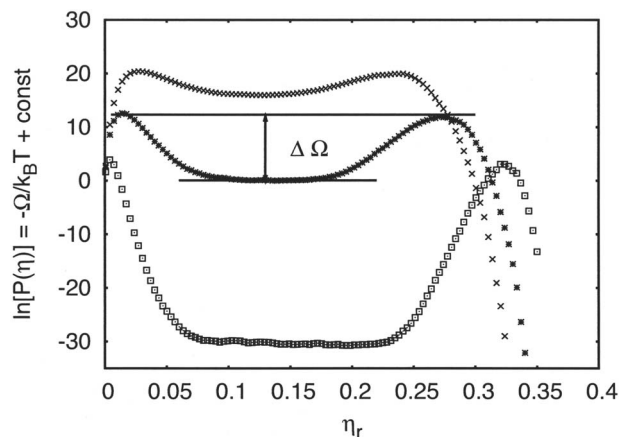


FIG. 2. Grand potential  $\ln[P(\eta_r)]$  for spherocylinders of aspect ratio  $L/D=5$  at sphere fugacities  $z_s=1.0125$  (crosses),  $1.0625$  (stars), and  $1.175$  (squares).  $\Delta\Omega$  indicates the height of the grand potential barrier between the coexisting phases.

$$\text{acc}(N_r \rightarrow N_r + 1) = \min \left[ 1, \frac{z_r n_s! 4\pi V e^{-\beta\Delta E}}{(V_{dz} z_s)^{n_s} m(N_r + 1)} \right], \quad (21)$$

if  $n_s < m$  and 0 otherwise. Here  $n_s$  is the number of spheres which need to be removed to produce a void, in which the spherocylinder can be inserted. If only one spherocylinder is inserted and no spheres are removed, the acceptance probability is reduced to

$$\text{acc}(N_r \rightarrow N_r + 1) = \min \left[ 1, \frac{z_r 4\pi V}{N_r + 1} e^{-\beta\Delta E} \right]. \quad (22)$$

## B. Phase boundaries from grand canonical simulations

We determined the phase boundaries from the probability distribution  $P(N_r)$ , which is the probability to observe  $N_r$  rods in the mixture for given chemical potentials  $\mu_r$  and  $\mu_s$ . For a given value of  $\mu_s$ , we searched for the value of  $\mu_r$  at which the distribution is bimodal. However, the simulations need not be performed right at the coexistence chemical potential (which is usually not known beforehand). In fact, the chemical potential can be set to any value  $\mu_r^{\text{sim}}$  and then renormalized to coexistence via

$$\ln[P_{\mu_r}(N_r)] = \ln[P_{\mu_r^{\text{sim}}}(N_r)] + (\mu_r - \mu_r^{\text{sim}})N_r, \quad (23)$$

such that the areas under the two peaks in  $P(N_r)$  are equal.<sup>22</sup> We used the successive umbrella sampling method<sup>16</sup> to determine  $P(N_r)$ . This technique allowed us to sample regions between the two bulk phases where  $P(N_r)$  is very low.

Figure 2 shows the logarithm of the probability distribution  $P(\eta_r)$  as a function of the rod volume fraction  $\eta_r = N_r v_r / V$  with  $v_r = \pi D^3(2 + 3L/D)/12$ , which—up to an additive constant—is equal to the grand potential of the system. The locations of the maxima of the peaks are the bulk volume fractions of rods at coexistence. For a large fugacity  $z_s$  (squares), and hence a large concentration of spheres, there are two clearly separated peaks indicating a phase transition which is strongly of first order. With decreasing concentration of spheres (stars and crosses) the effective attraction

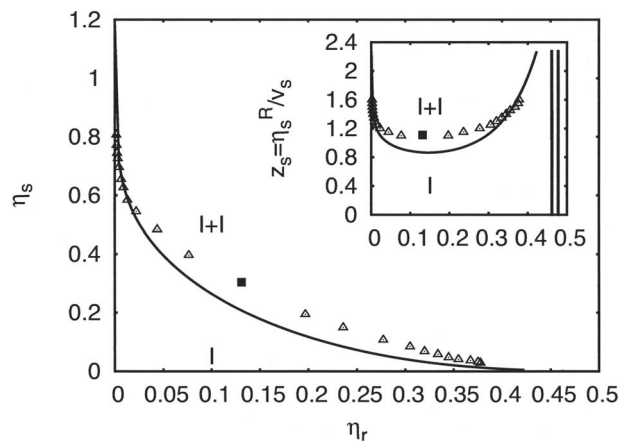


FIG. 3. Bulk phase diagram for a mixture of spherocylinders with aspect ratio  $L/D=3$  and spheres of diameter  $D$ . The solid lines are predictions of the free volume theory. The filled square marks the critical point. The inset shows the phase diagram in the  $(z_s, \eta_r)$ -plane. The almost vertical lines in the inset indicate the coexistence region of the isotropic-nematic transition.

between the rods becomes weaker. Hence the peaks broaden and move closer until eventually the critical point is reached.

Figure 1 shows a typical configuration at coexistence. Due to the periodic boundaries two slabs separated by two interfaces have formed.

In Fig. 2 one can also clearly see that an advanced biasing scheme such as successive umbrella sampling is necessary to bridge the huge differences in probabilities between the pure bulk states and the states in the two-phase coexistence region (which show up via a horizontal part of the  $\Omega$  versus  $\eta_r$  curve, since a change of  $\eta_r$  just amounts to a change of the sizes of the gas-like and liquid-like domains, without changing the areas of the interfaces between them).

## IV. RESULTS

### A. Bulk

#### 1. Phase diagram

The phase diagram is presented choosing the fugacity of the spheres and the rod volume fraction as variables. The fugacity  $z_s$  is related to the sphere reservoir volume fraction via  $\eta_s^R = z_s v_s$ , where  $v_s = \pi D^3/6$  is the volume of a sphere. Explicit implementation of the spheres allows an easy transformation into the frame of  $(\eta_s, \eta_r)$ , where  $\eta_s$  is the sphere volume fraction in the system. In the free volume theory the actual concentration of spheres follows as  $\eta_s = \alpha \eta_s^R$ , with  $\alpha$  from Eq. (17).

Figures 3 and 4 show phase diagrams for mixtures of rods with aspect ratios  $L/D=3$  and 5 and spheres. The solid lines are the free volume theory predictions. The single phase, the isotropic mixture of rods and spheres, is marked “I.” The region of the phase diagram, where the gas-like and liquid-like isotropic phases coexist, is named “I+I.” The two almost vertical lines are theoretical predictions for the phase boundaries of the isotropic-nematic transition.<sup>23</sup>

Since the free volume theory is based upon a mean-field approximation, and fluctuations, which are especially relevant near the critical point, are ignored, we expect its predictions to deviate from the simulation results there. Away

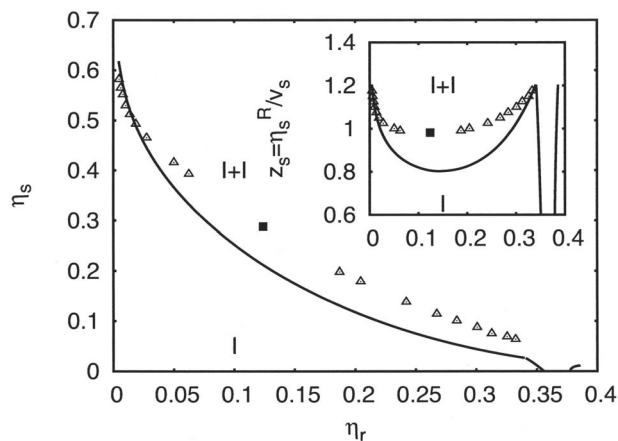


FIG. 4. Bulk phase diagram for a mixture of spherocylinders with aspect ratio  $L/D=5$  and spheres of diameter  $D$ . The solid lines are predictions of the free volume theory. The filled square marks the critical point. The inset shows the phase diagram in the  $(z_s, \eta_r)$ -plane. The almost vertical lines in the inset indicate the coexistence region of the isotropic-nematic transition.

from the critical point the predictions of the free volume theory approach the simulation results. As anticipated, the theory underestimates the volume fraction of spheres in the liquid phase considerably. This is due to the fact that the depletion forces change the local structure of the fluid,<sup>24</sup> an effect which is not included in the calculations of the free volume accessible to spheres. On the gas-branch of the coexistence region, where the amount of rods is negligible, the theoretical predictions agree well with the simulation results.

Figure 5 shows a comparison of our results with the data obtained in previous computer simulations on the fluid-fluid separation by Bolhuis *et al.*<sup>14</sup> (open squares). The errorbars of their data are  $\Delta \eta_r \sim 0.02$ . Thus, the results do not coincide within the errorbars. We attribute the difference to the small system sizes which were accessible at that time (1997). No estimate for the critical point could be obtained from their work.<sup>14</sup>

The results presented here are of high accuracy: The errorbars are smaller than the symbols. The main sources of error are finite size effects and insufficient sampling of the

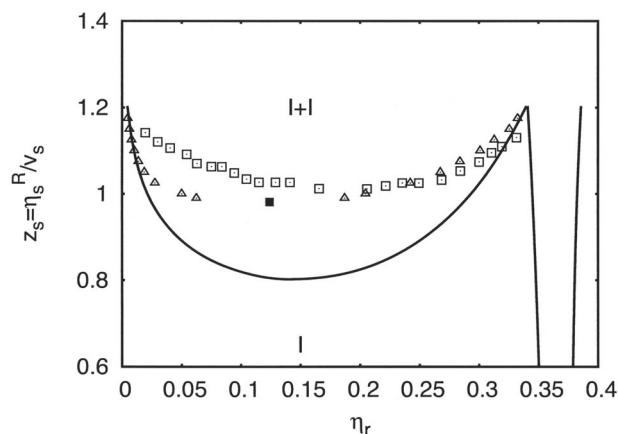


FIG. 5. Comparison of the bulk phase diagram for a mixture of spherocylinders with aspect ratio  $L/D=5$  and spheres of diameter  $D$  to previous work. The open triangles are the results of the present work, the filled square marks the critical point. The open squares are the data obtained by Bolhuis *et al.* (Ref. 14). The solid lines are predictions of the free volume theory.

grand potential hypersurface perpendicular to the reaction coordinate (i.e., the packing fraction of rods). In order to check for the quality of sampling, we repeated our simulations for several different chemical potentials and different values of accuracy thresholds in the successive umbrella sampling. From this we estimate the error on the coexistence volume fractions to be  $\Delta \eta_r = \pm 0.002$ .

Finite size effects enter in two ways: (1) At coexistence the system forms slab configurations with two interfaces (due to the periodic boundaries). If  $L_z$  is too small, the interfaces interact. Away from the critical point, we ruled out this contribution by increasing  $L_z$  such that a plateau appeared between the peaks in  $P(\eta_r)$ . (2)  $P(\eta_r)$  depends on the lateral box size, because the spectrum of capillary waves on the interfaces is cut off for wavelengths larger than the box. This effect is negligible far away from the critical point, too, because the interfacial tension there is large and the effects of capillary waves are very weak. However, close to the critical point a finite size scaling analysis becomes necessary. In fact, the two effects are then just two aspects of the same property, the diverging correlation length. We discuss this issue further in Sec. IV A 2.

Close to the isotropic-nematic transition, the simulations cannot be equilibrated properly with the methods used here. For accurate grand canonical simulations of the IN transition more advanced biasing techniques are necessary.<sup>25</sup> A study of this part of the phase diagram is beyond the scope of the present work however.

## 2. Finite size scaling

As explained above,  $P(\eta_r)$  depends on system size. This is, however, not a drawback but an advantage, because the finite size effects can be used in order to locate the critical point of isotropic-isotropic demixing. One can construct quantities which are independent of system size at the critical point. One possible choice<sup>22,26</sup> of such a quantity is the cumulant ratio  $U_4 = \langle m^4 \rangle / \langle m^2 \rangle^2$  with  $m = \eta_r - \langle \eta_r \rangle$ . When  $U_4$  is plotted versus  $z_s$  close to the critical point for different system sizes, the intersection point marks the critical point. Figure 6 shows that the critical sphere fugacity for spherocylinders with aspect ratio  $L/D=3$  is  $z_s^c = 1.109 \pm 0.001$ .

Figure 7 shows the difference in packing fraction  $\eta_r^l - \eta_r^g$  versus the “relative distance from the critical point”  $z_s/z_s^c - 1$  (circles for  $L/D=3$  and diamonds for  $L/D=5$ ). The upper line in the graph is proportional to  $(z_s/z_s^c - 1)^{\beta_{\text{Ising}}}$ , where  $\beta_{\text{Ising}} = 0.326$  is the critical exponent of the order parameter in the Ising model. Clearly, the critical point is of the Ising universality class.

## 3. Interfacial tension

In the transition region where the gas-like phase transforms into the liquid-like phase and vice versa, a grand potential barrier  $\Delta \Omega$  needs to be crossed (indicated in Fig. 2).  $\Delta \Omega$  is related to the interfacial tension via

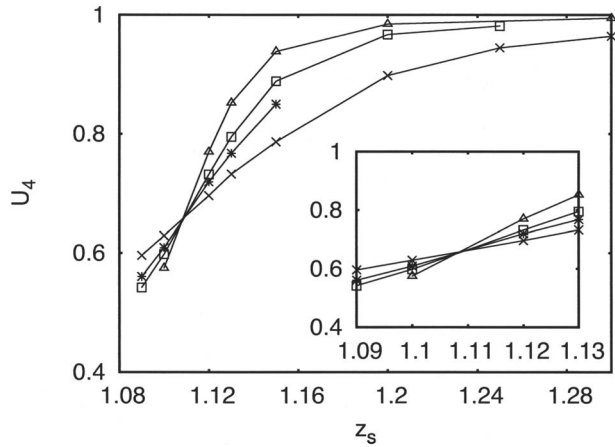


FIG. 6. Cumulant ratio  $U_4$  as a function of the sphere fugacity close to the critical point for box lengths  $L_x=9D$  (crosses),  $12D$  (stars),  $14D$  (squares), and  $18D$  (triangles). Spherocylinders aspect ratio is  $L/D=3$ . The inset shows a magnified plot of the region near the intersection point.

$$\gamma \equiv \lim_{L_x \rightarrow \infty} \frac{\Delta\Omega}{2L_x^2}, \quad (24)$$

where  $L_x^2$  is the area of the interface and the factor  $1/2$  accounts for the two interfaces, which are present due to the periodic boundary conditions.<sup>27</sup> Figure 7 shows values of the interfacial tension as a function of the “relative distance from the critical point”  $z_s/z_s^c - 1$  (triangles for  $L/D=3$  and squares for  $L/D=5$ ). The lower line in the graph indicates  $(z_s/z_s^c - 1)^{2\nu_{\text{Ising}}}$ , where  $2\nu_{\text{Ising}}=1.26$  is the critical exponent for the interfacial tension in the three dimensional (3D) Ising model.

## B. Confinement

### 1. Phase diagram

Now we consider the behavior of the mixture confined between two hard walls at distance  $d$ . Figures 8 and 9 show the phase diagrams for rod aspect ratios  $L/D=3$  and 5. The distance between the walls is  $d/D=3L/D$ . Demixing in confinement occurs at larger sphere fugacities than in the bulk.

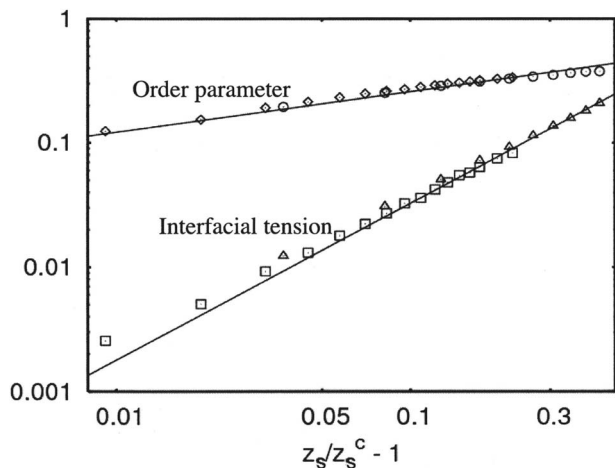


FIG. 7. Order parameter ( $\eta_r^c - \eta_s^c$ ) (circles and diamonds) and interfacial tension  $\gamma$  (triangles and squares) vs “relative distance from the critical point”  $z_s/z_s^c - 1$ . Spherocylinders aspect ratios are  $L/D=3$  (triangles and circles) and 5 (squares and diamonds). The solid lines correspond to the Ising power-law-behavior with exponents  $\beta_{\text{Ising}}=0.326$  and  $2\nu_{\text{Ising}}=1.26$ .

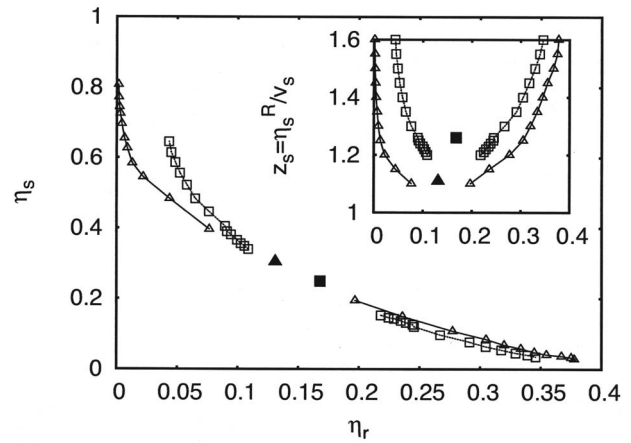


FIG. 8. Phase diagram for a mixture of spherocylinders with aspect ratio  $L/D=3$  and spheres of diameter  $D$  between two hard walls at distance  $d/D=3L/D$  (squares) compared to the bulk values (triangles). The filled symbols mark the critical points. The inset shows the phase diagram in the  $(z_s, \eta_r)$ -plane. The symbols show “raw data” for one box dimension  $L_x=12D$  only, and thus the curves marking the peaks of  $P(\eta_r)$  do not join at the critical points [“finite size tails” (Ref. 22)]. The lines serve to guide the eyes.

Also the chemical potential of the rods at coexistence is higher than in the bulk. The gas-like phase is shifted to larger rod volume fractions. The amount of spheres in the system is smaller than in the bulk at the same fugacity. The large increase of the concentration of rods in the gas-like phase distinguishes this system clearly from the behavior of the Asakura-Oosawa-Vrij model in confinement.

We also performed a finite size scaling analysis in confinement to see how the critical point is shifted (Fig. 10). Table I lists the results in comparison to the bulk results.

The relative shift in  $\eta_r^c$ , which we observe for rods with aspect ratio  $L/D=5$ , is larger than the one of rods with aspect ratio  $L/D=3$ , though the relative shift in  $z_s^c$  behaves the other way around. The second effect is due to the ordering of the spheres close to the walls. Thus, its relative decrease on

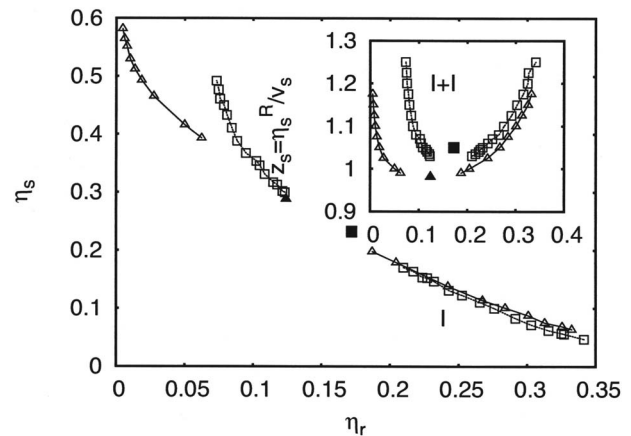


FIG. 9. Phase diagram for a mixture of spherocylinders with aspect ratio  $L/D=5$  and spheres of diameter  $D$  between two hard walls at distance  $d/D=3L/D$  (squares) compared to the bulk values (triangles). The filled symbols mark the critical points. The inset shows the phase diagram in the  $(z_s, \eta_r)$ -plane. The symbols show “raw data” for one box dimension  $L_x=20D$  only, and thus the curves marking the peaks of  $P(\eta_r)$  do not join at the critical points [“finite size tails” (Ref. 22)]. The lines serve to guide the eyes.

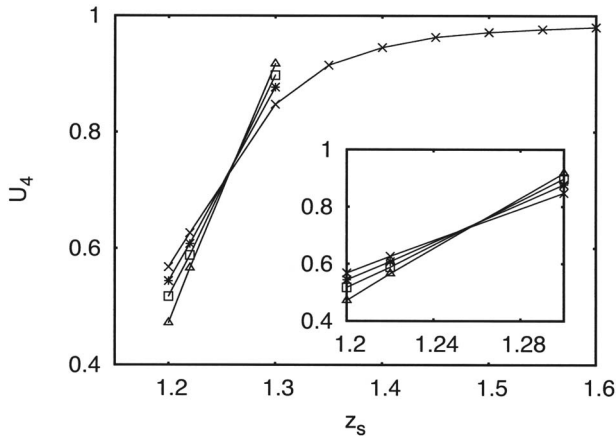


FIG. 10. Cumulant ratio  $U_4$  as a function of the sphere fugacity close to the critical point for box lengths  $L_r=12D$  (crosses),  $15D$  (stars),  $18D$  (squares), and  $21D$  (triangles) between two hard walls at distance  $d/D=3L/D$ . Aspect ratio  $L/D=3$ . The inset shows a magnified plot of the region near the intersection point.

increase of the rods' aspect ratio is plausible, since, in terms of the sphere diameter, the distance between the walls increases.

The shift in  $\eta_r^c$  is caused by the wall-induced layering of the rods. Because of orientational ordering, this effect is much stronger than, e.g., the shift in the Asakura-Oosawa-Vrij model, which is due to positional ordering.<sup>28</sup> Close to the wall the rods are preferably oriented parallel to the wall ("parallel anchoring"). Therefore, their concentration is much higher than in the isotropic bulk.

Obviously, it would be very interesting to investigate how the critical point depends on the wall separation  $d$ . This is unfortunately currently too demanding computationally. One week of CPU time on a Pentium 4, 2.60 GHz was needed to compute one density distribution in the  $(3L \times 3L \times 3L)$ -box, and one month of CPU time for the  $(5L \times 5L \times 5L)$ -box. Hence, a systematic study of the crossover from 3D to two dimensional (2D) system would require very large computational effort.

Anyway, we expect that for any finite film thickness  $d$  the critical behavior of the isotropic-isotropic phase separation belongs to the 2D Ising universality class, since a critical divergence of the correlation length can occur in the two directions parallel to the walls only. However, for not too small  $d$  this 2D-character of criticality can be detected only very close to the critical point. For sufficiently small wall separations, however, we expect that no isotropic-isotropic phase separation will be observed in thermal equilibrium; since the walls induce alignment of the rods, the nematic-isotropic transition will take over. Considering a phase diagram with  $d$  as a control parameter, we speculate that the line

TABLE I. Critical point in the bulk and in confinement to slit-pore of width  $d/D=3L/D$ .

$L/D$	$z_{s,\text{conf}}^c$	$\eta_{r,\text{conf}}^c$	$z_{s,\text{bulk}}^c$	$\eta_{r,\text{bulk}}^c$
3	$1.26 \pm 0.01$	$0.168 \pm 0.002$	$1.109 \pm 0.001$	$0.131 \pm 0.002$
5	$1.05 \pm 0.01$	$0.172 \pm 0.002$	$0.981 \pm 0.001$	$0.124 \pm 0.002$

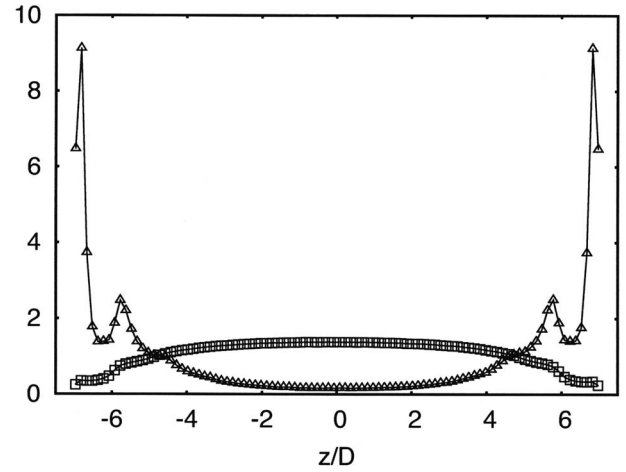


FIG. 11. Density distribution of rods (triangles) and spheres (squares) normalized by their overall densities in the gas-like phase between two hard walls at distance  $d/D=3L/D$ . Aspect ratio  $L/D=5$ . Corresponding sphere fugacity is  $z_s=1.1$ .

of critical points of the isotropic-isotropic phase separation will terminate at a critical endpoint at the first-order nematic-isotropic transition line.

## 2. Order parameter profiles

The walls change the structural properties of the gas- and liquid-like phases of rods. Here we show data from simulations in the  $NVT$ -ensemble, where the volume of the system as well as the numbers of rods and spheres are fixed. The number of particles was chosen to match the coexistence values determined in the grand canonical ensemble. Although in principle finite size effects are different in the canonical and grand canonical ensemble,<sup>22</sup> far enough away from the critical point this difference can safely be neglected.

To study the anchoring effects of the walls, we define the nematic order parameter  $S$  and the biaxiality parameter  $\xi$ .  $S$  is the largest absolute eigenvalue<sup>29</sup> of the matrix

$$\mathbf{Q} = \frac{1}{2\tilde{N}_r} \sum_{i=0}^{\tilde{N}_r} (3\mathbf{u}^i \mathbf{u}^i - \mathbf{I}), \quad (25)$$

where  $\mathbf{u}^i$  is a unit vector in the direction of the orientation of the rod  $i$  and  $\mathbf{I}$  is the identity matrix. We divide the space between the walls into thin slices, so  $\tilde{N}_r$  is the number of rods in such a slice at the distance  $z/D$  from the middle of the simulation box. (Note that many authors use the largest eigenvalue instead of the eigenvalue with the largest absolute value, which leads to different results in the case of uniaxial surface ordering.)  $S$  indicates if there is a preferred direction in the system and how strongly the rods are oriented with respect to it. The eigenvector to this eigenvalue is called director. If  $S$  is zero, the phase is completely isotropic. If  $S$  is unity, all rods are aligned parallel to the director. If  $S$  is negative, they lie perpendicular to the director. The biaxiality measure  $\xi$  is half of the difference of the other two eigenvalues of the matrix  $\mathbf{Q}$ . It shows whether there is another preferred direction in the plane perpendicular to the director.

Figures 11 and 12 show the density distributions of rods with aspect ratio  $L/D=5$  and spheres between walls at a

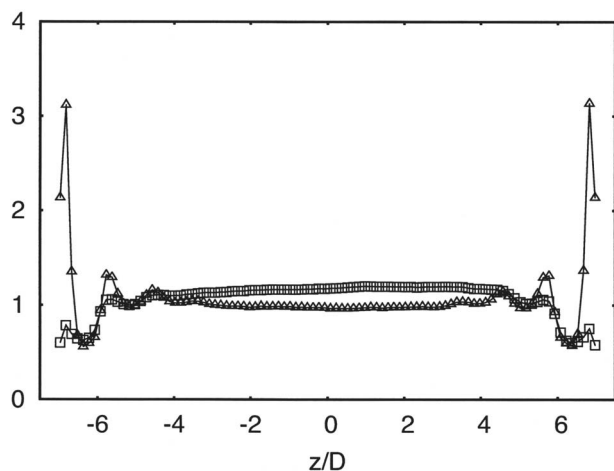


FIG. 12. Density distribution of rods (triangles) and spheres (squares) normalized by their overall densities in the liquid-like phase between two hard walls at distance  $d/D=3L/D$ . Aspect ratio  $L/D=5$ . Corresponding sphere fugacity is  $z_s=1.1$ .

distance  $d/D=3L/D$ . Figure 11 shows the gas-like phase, Fig. 12 the corresponding liquid-like phase at coexistence. The overall densities are approximately the positions of the peaks of the probability distribution  $P(\eta_r)$  from the grand canonical simulation at sphere fugacity  $z_s=1.1$ .

Figures 13 and 14 show the corresponding profiles of the nematic order parameter  $S$  and of the biaxiality parameter  $\xi$  in the gas- and liquid-like phases, respectively.

The positional as well as the orientational order of rods are clearly visible in the liquid- as well as in the gas-like phases. The range of the induced effects is of the order of the rod length, which is short in comparison to the chosen distance between the walls. In the middle of the system the order parameters reach their bulk values. The spheres are pushed away from the walls. This effect is also of the order of the rod length in both phases.

## V. DISCUSSION AND SUMMARY

We have presented simulation results on the phase diagram of mixtures of hard spherocylinders and “penetrable

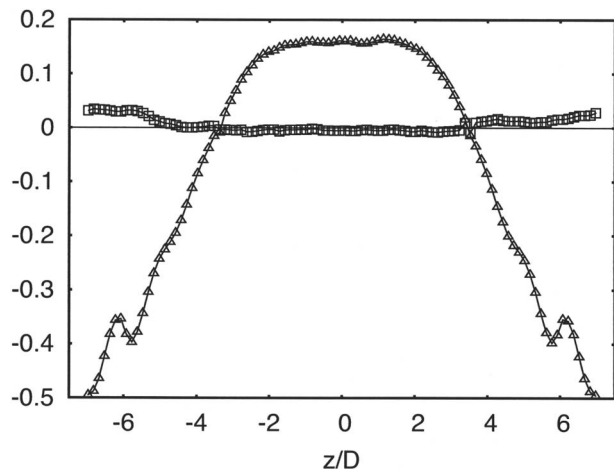


FIG. 13. Nematic order  $S$  (triangles) and biaxiality  $\xi$  (squares) parameter distributions in the gas-like phase between two hard walls at distance  $d/D=3L/D$ . Aspect ratio  $L/D=5$ . Corresponding sphere fugacity is  $z_s=1.1$ .

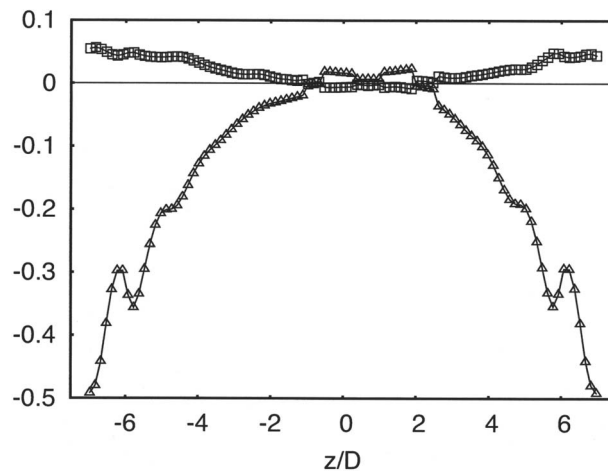


FIG. 14. Nematic order  $S$  (triangles) and biaxiality  $\xi$  (squares) parameter distributions in the liquid-like phase between two hard walls at distance  $d/D=3L/D$ . Aspect ratio  $L/D=5$ . Corresponding sphere fugacity is  $z_s=1.1$ .

hard” spheres in the bulk and in confinement. We hope that these results are useful for experimental investigations of suspensions of viruses and polymers.

We have studied isotropic-isotropic demixing by simulations in the grand canonical ensemble. In order to access states of high free energy we used the successive umbrella sampling method. The resulting phase boundaries were compared to the free volume theory. We extracted the critical point from an analysis of the cumulants of the order parameter distribution. The free volume theory works well far away from the critical point, but, as expected, underestimates the concentrations at the critical point.

In the bulk the system is very similar to the Asakura-Oosawa-Vrij model. In particular, we showed that its behavior on approach to the critical point falls into the Ising universality class. In confinement, however, the orientational degrees of freedom play a role. As the rods anchor parallel to the wall, the gas-like branch of the coexistence region moves to higher colloid (rod) volume fractions than in the Asakura-Oosawa-Vrij model. The walls induce a much larger shift in the critical colloid (rod) volume fraction than they do for spherical colloids.

## ACKNOWLEDGMENTS

We would like to thank Jürgen Horbach, Richard Vink, and Peter Virnau, for helpful suggestions. This work was part of the priority program SFB Tr6 (Project No. D5) of the German Research Association (DFG). It was partially funded by the DFG Emmy-Noether-Program, the MWFZ Mainz. It has also been supported by the European Commission under the Sixth Framework Program through integrating and strengthening the European Research Area. Contract No. SoftComp VP-06/109. We thank the Forschungszentrum Jülich for CPU time on the JUMP.

<sup>1</sup>T. T. Hebert, *Phytopathology* **53**, 362 (1963).

<sup>2</sup>Z. Dogic and S. Fraden, *Curr. Opin. Colloid Interface Sci.* **11**, 47 (2006).

<sup>3</sup>K. Kang, M. Lettinga, Z. Dogic, and J. K. G. Dhont, *Phys. Rev. E* **74**, 026307 (2006).

<sup>4</sup>J. K. G. Dhont, M. Lettinga, Z. Dogic, T. Lenstra, H. Wang, S. Rathgeber,

- P. Carletto, L. Willner, H. Frielinghaus, and P. Lindner, *Faraday Discuss.* **123**, 157 (2003).
- <sup>5</sup>T. Lenstra, Z. Dogic, and J. Dhont, *J. Chem. Phys.* **114**, 10151 (2001).
- <sup>6</sup>M. Lettinga and J. Dhont, *J. Phys.: Condens. Matter* **16**, S3929 (2004).
- <sup>7</sup>F. Oosawa and S. Asakura, *J. Chem. Phys.* **22**, 1255 (1954).
- <sup>8</sup>A. Vrij, *Pure Appl. Chem.* **48**, 471 (1976).
- <sup>9</sup>Y. Chen and K. Schweizer, *J. Chem. Phys.* **117**, 1351 (2002).
- <sup>10</sup>Y. Chen and K. Schweizer, *J. Phys. Chem. B* **108**, 6687 (2004).
- <sup>11</sup>A. Cuetos, B. Martinez-Haya, S. Lago, and L. Rull, *Phys. Rev. E* **75**, 061701 (2007).
- <sup>12</sup>H. N. W. Lekkerkerker and A. Stroobants, *Nuovo Cimento D* **16**, 949 (1994).
- <sup>13</sup>W. Li and H. R. Ma, *Eur. Phys. J. E* **16**, 225 (2005).
- <sup>14</sup>P. G. Bolhuis, A. Stroobants, D. Frenkel, and H. N. W. Lekkerkerker, *J. Chem. Phys.* **107**, 1551 (1997).
- <sup>15</sup>S. V. Savenko and M. Dijkstra, *J. Chem. Phys.* **124**, 234902 (2006).
- <sup>16</sup>P. Virnau and M. Müller, *J. Chem. Phys.* **120**, 10925 (2004).
- <sup>17</sup>M. Cotter, *J. Chem. Phys.* **66**, 1098 (1977).
- <sup>18</sup>R. van Roij, *Eur. J. Phys.* **26**, S57 (2005).
- <sup>19</sup>R. L. C. Vink and T. Schilling, *Phys. Rev. E* **71**, 051716 (2005).
- <sup>20</sup>T. Biben, P. Bladon, and D. Frenkel, *J. Phys.: Condens. Matter* **8**, 10799 (1996).
- <sup>21</sup>R. L. C. Vink and J. Horbach, *J. Chem. Phys.* **121**, 3253 (2004).
- <sup>22</sup>D. P. Landau and K. Binder, *A Guide to Monte Carlo Simulations in Statistical Physics* (Cambridge University Press, Cambridge, 2000).
- <sup>23</sup>R. Tuinier, T. Taniguchi, and H. H. Wensink, *Eur. Phys. J. E* **23**, 355 (2007).
- <sup>24</sup>T. Schilling, S. Jungblut, and M. A. Miller, *Phys. Rev. Lett.* **98**, 108303 (2007).
- <sup>25</sup>R. Vink, S. Wolfsheimer, and T. Schilling, *J. Chem. Phys.* **123**, 074901 (2005).
- <sup>26</sup>K. Binder, *Z. Phys. B: Condens. Matter* **43**, 119 (1981).
- <sup>27</sup>K. Binder, *Phys. Rev. A* **25**, 1699 (1982).
- <sup>28</sup>R. Vink, K. Binder, and J. Horbach, *Phys. Rev. E* **73**, 056118 (2006).
- <sup>29</sup>R. J. Low, *Eur. J. Phys.* **23**, 111 (2002).